Computational and Theoretical Chemistry 1236 (2024) 114554

Contents lists available at ScienceDirect

Computational and Theoretical Chemistry

journal homepage: www.elsevier.com/locate/comptc

Solvation effects on the excitation dynamics, structural and photorelaxation, quantum chemical investigation, and photophysical properties of 2D p-expanded quinoidal terthiophene (2DQTTs): Outlook from Ab-initio calculations

Thomas O. Magu [a,b,c,d,*], Terkumbur E. Gber [e,c], Rasaq A. Adams [b], MaryAnn A. Odume [c], Sunday S. Ikiensikimama [a]

[a] World Bank Africa Center of Excellence, Center for Oilfield Chemicals Research (ACE-CEFOR), University of Port Harcourt, Nigeria
[b] Department of Chemistry, University of Florida Gainesville, FL 32611, United States
[c] Department of Pure and Applied Chemistry, University of Calabar, Calabar, Nigeria
[d] Key Laboratory of Green Printing, Beijing National Laboratory for Molecular Science, Institute of Chemistry, University of Chinese Academy of Sciences, Beijing 100190, China
[e] Department of Research Analytics, Saveetha Dental College and Hospitals, Saveetha Institute of Medical and Technical Sciences Saveetha University, Chennai India

ARTICLE INFO

Keywords:
Terthiophenes
structure
excitation
relaxation
photovoltaic
DFT

ABSTRACT

All dyes have different degrees of absorption. The present study delves into the intricate interplay between solvation and the photophysical behaviors of 2D p-expanded quinoidal terthiophene (2DQTT) dye compounds represented as A3, A4, and A5. In this study, a comprehensive investigation is presented, elucidating how solvation impacts excitation dynamics, ground and excited state geometry, photophysical characteristics. and photorelaxation dynamics of 2DQTTs. The energy gap data shows that the energies of the compounds increased in polar mediums and were greater for compound A3 which had ΔE values of 3.5227 eV in water, and 3.5225 eV in DMSO while compound A5 had the highest ΔE in all phases, with a ΔE value of 3.5453 eV in EtOH. Relaxation of the compounds leads to changes in the bonds and structural conformation of the 2D P-expanded quinoidal terthiophene (2DQTT) compounds as the compounds de-excite back to a lower energy level, and the photon causes a change in structural bonding (Stokes shift) in the heteroatoms which was taken into consideration. This manuscript not only advances our fundamental understanding of the interactions between solvation and molecular structure but also provides valuable insights into optimizing the performance of 2DQTT in optoelectronic devices as the compounds display a high absorption band in all phases, especially in water medial with compound A3, A4 and A5 recording absorbances of 785.32 nm, 787.13 nm, and 786.78 nm respectively, a high light harvesting efficiency LHE, great electron exciton energy and an injecting capacity (ΔG_{inject}) greater than 0.20 eV in all phases. This work contributes significantly to the design and application of novel materials for next-generation optoelectronic technologies hence we hope that experimental research tests the studied compound towards the mentioned application.

1. Introduction

Pi-Quinoidal terthiophene is an oligomer of the heterocycle thiophene. Quinoidal terthiophene is a type of organic compound that belongs to the family of terthiophenes. It is characterized by its unique extended quinoidal structure composed of three thiophene rings, which refers to the presence of alternating single and double bonds along the molecule's backbone [1]. This structure provides quinoidal terthiophene derivatives with unique electronic and optical properties. Quinoidal terthiophene has gained significant attention in the field of organic electronics due to its potential applications in various devices, such as organic field-effect transistors (OFETs), organic solar cells, and organic light-emitting diodes (OLEDs) [2,3]. Its quinoidal structure allows for efficient charge transport and enhanced pi-conjugation, which

* Corresponding author.
E-mail address: thomas.magu@unical.edu.ng (T.O. Magu).

https://doi.org/10.1016/j.comptc.2024.114554
Received 23 December 2023; Received in revised form 4 March 2024; Accepted 10 March 2024
Available online 26 March 2024

are desirable properties, including strong absorption in the visible region of the electromagnetic spectrum. This makes it suitable for light-harvesting applications in solar cells and as an active material in OLEDs, where it can emit light when an electric current is applied. Its potential application makes it an exciting area of research in the field [4]. OLEDs and solar cells use organic compounds to construct electronic devices that emit light by converting sunlight into a source of power. These devices are portable, flexible and cost-efficient compared to their inorganic counterparts [5]. OLEDs use organic materials to produce light when electric current passes through them while organic solar cells have the ability of organic materials to convert sunlight to electricity. The ability to use these organic molecules for specified electronic attributes has given rise to higher levels of visual technology and renewable sources of light [6].Fig 1.

Photophysical and photorelaxation dynamics are two important aspects of the field of photochemistry. Both of these methods involve the study of molecular processes involved in the absorption of light, but they differ in their specific focus and mechanisms [7]. Photophysical dynamics primarily address immediate events that occur after a molecule absorbs light. This includes processes such as internal conversion, intersystem crossing, and fluorescence. Internal conversion involves the nonradiative relaxation of a molecule's electronic excited state to a lower energy state within the same electronic state. The intersystem addresses the transition from one electronic state to another with a different spin multiplicity. Finally, fluorescence is the emission of light by a molecule as it returns to its ground state from an excited state [8,9]. In contrast, photo relaxation dynamics involve the longer-term processes that occur after the initial photophysical events.

The manipulation of molecular properties through solvation is a fundamental phenomenon that plays a crucial role in various chemical and physical processes. In the realm of photoactive materials, understanding the intricate interplay between molecular structure and solvent environment is of paramount importance for optimizing the performance of optoelectronic devices [10]. Prior research endeavors have explored the interplay between solvation and the optical properties of various organic semiconductors, shedding light on the mechanisms that govern their performance.

Several notable articles have contributed to the elucidation of solvation effects on the photophysical behavior of organic materials. For instance, Rohman and coworkers [11] investigated the effect of a specific solvent on the photophysical behaivoir of substituted chromones (AMC and CyC) via quantitative estimations using the Lippert-Mataga relation, uni-parametric ET(30) and multi-parametric Kamlet–Taft and/or Catalán relations, with notable solvatochromic shifts in the emission peak estimated for CyC ($\Delta\lambda = 130$ nm) in comparison with AMC ($\Delta\lambda = 53$ nm) and large bathochromic shifts in the fluorescence spectra of CyC (~130 nm) in comparison with AMC (~53 nm) which was rationalized on the basis of the large excited state dipole moment in CyC (~8.69 D) compared with AMC (~6.11 D).Additionally, the effects of solvent on the photophysical properties of synthesized ((E)-N-((E)-3-(4 (dimethylamino)phenyl) allylidene)-4-(trifluoromethyl) benzenamine (DPATB) and the detailed photophysics of the intramolecular charge transfer process have been explored on the basis of steady state absorption, fluorescence and time resolved spectroscopy in combination with density functional theory calculations by Nath et al [12]. The findings in their work showed that large solvent dependent fluorescence spectral shift and large calculated excited- state dipole moment clearly indicate that efficient charge transfer occurrs from the donor group to the acceptor moiety in the excited state of the Schiff base. Furthermore, Anshuman Mangalum [13] conducted a comprehensive spectroscopic study on a series of conjugated polymers and inter-chromophore interactions, highlighting the photophysical characterization and excited-state dynamics for biological sensor applications. Building upon these insights, Fengjiao Zhang et Chong-an Di [14] explored 2DQTTs as a

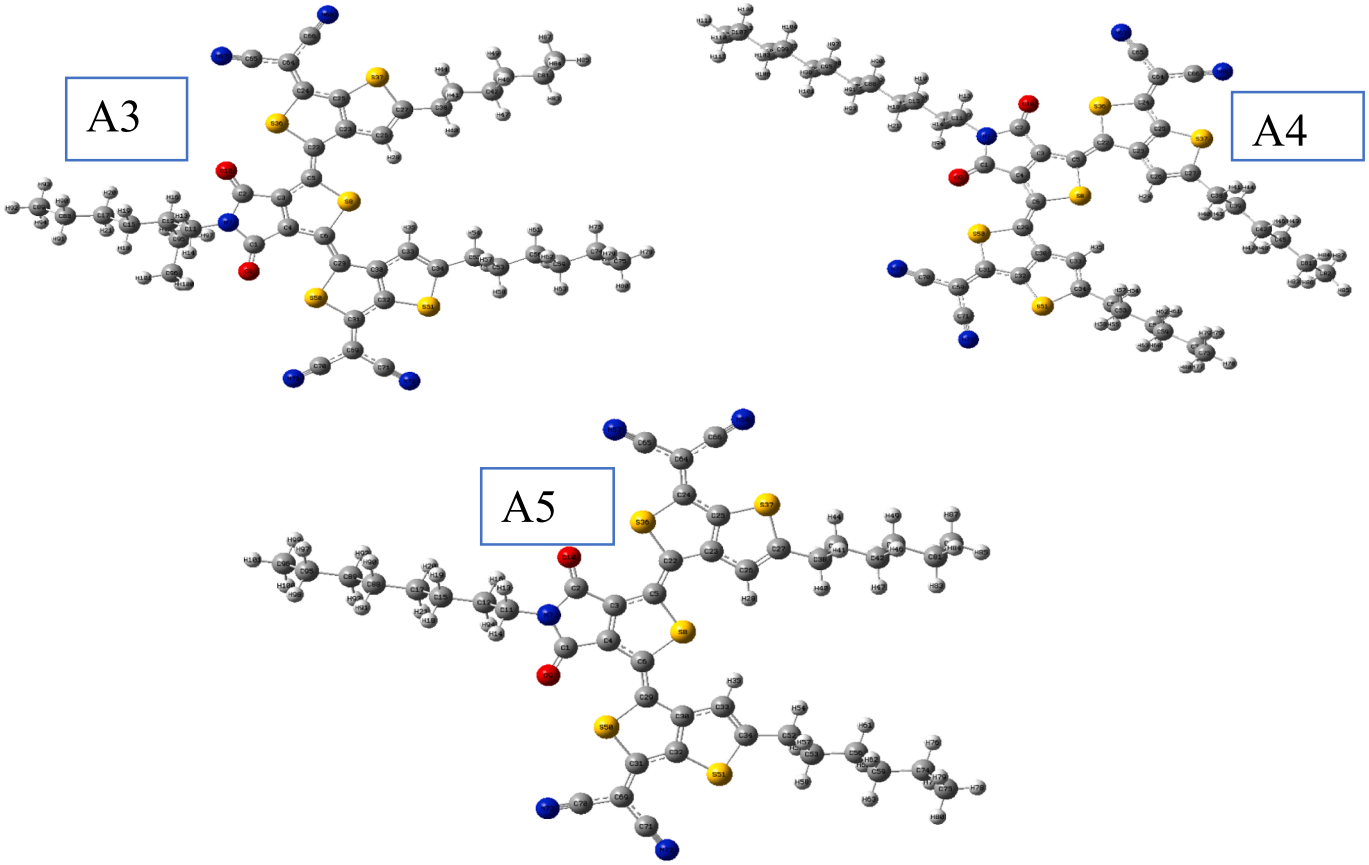

Figure 1. Structural presentation of the 2D p-expanded quinoidal terthiophene (2DQTT) compounds labelled A3, A4, and A5.

thermoelectric material with high charge carrier mobility, revealing an intriguing perspective for harnessing the 2DQTT material which they reported to have promising applications in flexible electricity generators and ultrathin solid cooling elements. Moreover, investigations by Zhang et al [15] focused on the design and characterization of novel small-molecule optoelectronic materials based on the thieno[3,4-b] thiophene core. This study explored the synthesis, structural properties, and optoelectronic behavior of these materials. The thieno[3,4-b] thiophene framework is chosen for its promising electronic properties, and this research aims to establish its potential for applications in various optoelectronic devices such as organic solar cells, light-emitting diodes, and photodetectors. This investigation sheds light on the structure-property relationships and performance of these materials, contributing to the advancement of organic electronics. Computational chemistry methods such as DFT have also aided in the development of 2D p-expanded quinoidal terthiophene. C. Zhang et al [16] reported the design and selective synthesis of 2D p-expanded quinoidal terthiophenes with proximal and distal regiochemistry for high performance n-channel organic thin-film transistors featuring high electron mobility, solution processability and ideal stability. They also stated in their paper that 2DQTT is the first among the QOTs that exhibits an electron mobility surpassing 1.0 $cm^2V^{-1}s^{-1}$ revealing the potential of its framework for constructing n-type organic semiconductors. Due to this high mobility, we have a high probability of 2DQTT undergoing solvation in different solvents to produce organic solar devices.

In light of these existing research endeavors, the present manuscript aims to contribute to the growing body of knowledge by investigating in detail the effects of solvation on the photophysical and photorelaxation dynamics of 2D p-expanded quinoidal terthiophenes (2DQTTs). Through a combination of computational simulations, theoretical analysis, electronic and stability analysis, nonlinear optics, electron hole analysis and relaxation florescence pathway analysis, we aim to unravel the intricate interplay between solvent interactions with various polarities and electronic and excitation processes within these materials. The insights gained from this study not only deepen our fundamental understanding of 2DQTTs but also offer valuable guidance for the design and optimization of next-generation organic electronic devices.

2. Methods

2.1. Experimental

The experimental design and synthesis of 2D P-expanded quinoidal terthiophene (2DQTT) compounds were previously reported by Fan et al [17]. Herein, we obtained the structures to theoretically investigate the photophysical and photorelaxation properties of the compounds as well as the effect of the solvent on the processes.

2.2. Computational methodology

Herein, we comprehensively investigated the photophysical and photorelaxation dynamics of 2D p-expanded quinoidal terthiophene (2DQTT) under various solvent conditions. The insights gained from these analyses contribute to a deeper understanding of the behavior of this molecule and its potential applications in optoelectronic devices. The molecular structures of 2D p-expanded quinoidal terthiophene (2DQTT) in the gas phase and in various solvents were subdued to local minima were the structure of (2DQTT) was sketch with Guass View 6.0.16 and optimized with Gaussian 16 software [18,19]. Solvent effects were accounted for using the polarizable continuum model (PCM) [20]. Long-range CAM-B3LYP/6-31+G(d,p). The DFT method was employed for this study in gas, water, DMSO, ethanol, and chloroform media. The Electronic excitation energies were determined using the CAM-B3LYP Coulomb attenuated functional because CAM-B3LYP provides the best overall performance [21,22].The resulting optimized geometry was used as the starting point for further investigations. The electronic properties of 2DQTTs were analysed by calculating their frontier molecular orbitals (HOMO and LUMO) and energy gap (HOMO-LUMO gap) as well as quantum reactivity descriptors to understand their electronic structure and potential for charge transfer using the Molecular orbitals using equations 1-6.

$$\Delta E = EHOMO - ELUMO \quad (1)$$

$$\sigma = \frac{1}{\eta} = \frac{1}{IP - EA} = \frac{1}{E_{LUMO} - E_{HOMO}} \quad (2)$$

$$\mu = -(IP + EA)/2 \quad (3)$$

$$\eta = (IP - EA)/2 \quad (4)$$

$$\chi = -\mu = 1/2IP + EA \quad (5)$$

$$\omega = \mu 2/2\eta \quad (6)$$

The Chemcraft 1.6 software package [23] was used to visualize the HOMO-LUMO plots. NBO analysis was conducted to gain insight into the electronic structure and intra-molecular interactions within 2DQTTs as well as the compound stability and electron delocalization in different solvents facilitated by the NBO 7.0 module [24] embedded in the Gaussian 16 software program [25] using equation 7.

$$\boldsymbol{E}(2) = \boldsymbol{\Delta Eij} = -\boldsymbol{qiF}2(\boldsymbol{ij})/\boldsymbol{Ei} - \boldsymbol{Ej} \quad (7)$$

where qi denotes the electron donor orbital occupancy, and Ei and Ej represent for the orbital energies of the donor and acceptor NBO orbitals respectively.

Nonlinear optical properties, including first hyperpolarizability, and dipole moment were computed to provide insights into the molecular stability and polarizability of 2DQTTs for nonlinear optical applications [26] using equations 8-10.

$$\alpha total = 1/3(\alpha xx + \alpha yy + \alpha zz) \quad (8)$$

$$\beta total = (\beta x + \beta y + \beta z)1/2 \quad (9)$$

where,

$\beta_x = \beta_{xxx} + \beta_{xyy} + \beta_{xzz}$
$\beta_y = \beta_{yyy} + \beta_{yzz} + \beta_{yxx}$
$\beta_z = \beta_{zzz} + \beta_{zxx} + \beta_{zyy}$

Hence the equation is written as

$$\beta total = [(\beta xxx + \beta xyy + \beta xzz)2 + (\beta yyy + \beta yzz + \beta yxx)2 + (\beta zzz + \beta zxx + \beta zyy)2]1/2 \quad (10)$$

Excited state properties were investigated in various solvents using time-dependent DFT (TD-DFT) calculations. UV/Vis excitation analyses were carried out to understand the electronic transitions responsible for the absorption spectra observed in different solvents. This involved computing the excitation energies, oscillator strengths, and transition dipole moments. Hole and electron distribution processes involved in photophysical and relaxation dynamics phenomena were analysed to understand charge carrier mobility and transport within the molecule as well as to comprehend the charge carrier recombination pathways and

lifetimes utilizing the TD-DFT methods [27]. Geometry optimizations were further performed on the relaxation of the compounds to obtain ground-state structures in the absence of solvent effects using the TD-SCF and CAM-B3LYP/6-31+G(d,p) DFT method, providing insights into the inherent conformational preferences of 2DQTTs, which were compared with the experimental geometries. The potential photovoltaic performance of 2DQTTs was assessed through calculations of exciton binding energies and charge transfer rates, considering different solvation environments utilizing the multiwfn 3.7 dev software suite developed by Lu and Chen [28].

3. Results and discussion

3.1 Molecular structure analysis

Solvent molecules can induce conformational changes in molecules, hence, influencing excited-state geometries and behavior. Geometry optimization was carried out to elucidate the structural characteristics of the 2D P-expanded quinoidal terthiophene (2DQTT) compounds labelled A3, A4 and A5 in the gas phase and the results were compared with experimental analysis to gain insights into the photochemical potentials of the compounds. The optimization analysis and the structural parameters including the bond labels and bond lengths of the studied structures were theoretically calculated by employing the CAM-B3LYP/6-31+G(d,p) level of theory while considering specific atom bonds made by the heteroatoms (N,O, and S) present in the molecules and the results are tabulated in Table 1. Additionally, the structural analysis of the compounds of interest (A3, A4 and A5) is of paramount importance for revealing the intricate relationships between molecular structure and optical behavior. It enables the rational design of materials with tailored photophysical properties and contributes to advancements in various technological and scientific fields as revealed by optoelectronic properties, such as absorption and emission wavelengths, quantum yields, and excited-state lifetimes [29]. Moreover, photorelaxation involves the relaxation of a molecule from an excited state back to the ground state [30]. Structural analysis can provide insights into the various relaxation pathways available to the molecule, including internal conversion, intersystem crossing, and radiative or non-radiative decay [31]. Hence, we focused on elucidating the structural composition of the compounds because computational methods often rely on accurate structural data to predict photophysical behavior. The length of a chemical bond within a compound is highly important for establishing diverse characteristics such as energy levels, reactivity patterns, and stability [32]. Moreover, it exerts a direct influence on the resilience and attributes of the chemical linkages between atoms. The bond length delineates the spatial separation between the nuclei of two atoms that are bound together within a molecule [33]. A diminished bond length signifies heightened strength in the connection between the atoms involved in the interaction. Herein, the analysis of the theoretical bond lengths, revealed that compound A3 exhibited an increase in bond length for all bonding interactions except for a slight decrease in N_{20} - C_{25} which had a theoretical bond length of 1.390 Å compared with the experimental value of 1.391 Å. In compound A5, the same trend was observed as the number of bonds increased in the theoretical investigations for all interactions except at N_{80} - C_{138} bond label, where a theoretical bond length of 1.389 Å was observed compared with the 1.397 Å recorded in the experimental data. Considering compound A4, we observed an alternating increase and decrease in the number of bonds. Notable increases were observed for S_{27} - C_{53}, S_{25} - C_{41}, N_{34} - C_{49}, and O_{31} - C_{40} with experimental and theoretical values of 1.748 Å and 1.782 Å, 1.758 Å and 1.782 Å, 1.135 Å and 1.158 Å, 1.179 Å and 1.208 Å respectively corresponding to the above bond labels. Moreover, a decrease in the bond length was observed for the S_{29} - C_{54}, N_{32} - C_{37}, and O_{30} - C_{37} bond labels. Analysing the structural parameters of the compounds herein provides insights into how the arrangement of atoms and bonds affects the electronic transitions and energy levels that drive these photophysical processes.

3.1. Electronic property investigation

3.1.1. Quantum parameters

In simple terms, the analysis of frontier molecular orbitals (FMOs) relies on comparing the energy difference between the highest occupied molecular orbital (HOMO), which serves as the electron donor orbital, and the lowest unoccupied molecular orbital (LUMO), which serves as the electron acceptor orbital [34]. These orbitals work together complementarily. The use of global quantum reactivity descriptors is crucial for understanding the electronic characteristics of a chemical entity. The idea behind assessing chemical reactivity through FMO analysis is that reactive species exhibit a smaller energy gap, indicating lower stability, compared to those with a larger energy gap, which implies greater stability [35]. According to Tjalling Koopman's mathematical approximations, the electron affinity (EA) and ionization energy (IP) of a given chemical species are related to the negative values of E_{LUMO} and E_{HOMO}, respectively. Moreover, global reactivity descriptors such as the electrophilicity index (ω), chemical softness (σ), electronegativity (χ), chemical potential (μ), and chemical hardness (η), obtained using the Koopmans theorem, serve as indicators of stability and reactivity. Generally, softer molecules exhibit greater reactivity than harder molecules because they readily donate electrons to acceptors [36]. The concepts describe the tendency of atoms or atom groups to donate and receive electrons, respectively. Additionally, hard molecules are characterized by a large energy gap, while soft molecules have a smaller energy gap. In this study, the stability and reactivity of the investigated compounds were assessed using the CAM-B3LYP/6-31+G(d,p) level of theory in the presence of four different solvents and the gas phase to a gain proper understanding of the 2D P-expanded quinoidal terthiophene (2DQTT) subsets (A3, A4, A5). Mathematically, the band gap and quantum reactivity parameters are presented in the methodology section, and the results displayed in Table 2. As observed from the computed results, the gas phase had a high HOMO which ranged from -7.0817 eV (A4) to -7.0834 eV (A3), and the LUMO values were highest when compared to those of the solvent media, which ranged from -3.5780 eV (A3) to -3.5791 eV (A5). The energy gaps for the compounds

Table 1
Theoretical and experimental bond length analysis of 2D P-expanded quinoidal terthiophene (2DQTT) dye compounds upon excitation, studied at the CAM-B3LYP/6-31+G(d,p) level of theory.

COMPOUNDS	A3			A4			A5	
	BOND DISTANCES (Å)			BOND DISTANCES (Å)			BOND DISTANCES (Å)	
Bond label	Experimental	Theoretical	BOND LABEL	Experimental	Theoretical	BOND LABEL	Experimental	Theoretical
S_{13} - C_{29}	1.766	1.782	S_{27} - C_{53}	1.748	1.782	S_{75} - C_{142}	1.706	1.724
S_{16} - C_{41}	1.771	1.782	S_{29} - C_{54}	1.747	1.724	S_{74} - C_{140}	1.774	1.782
N_{20} - C_{25}	1.391	1.390	S_{25} - C_{41}	1.758	1.782	S_{73} - C_{149}	1.770	1.782
S_{17} - C_{43}	1.708	1.724	N_{32} - C_{37}	1.396	1.389	N_{80} - C_{138}	1.397	1.389
S_{15} - C_{32}	1.713	1.724	O_{30} - C_{37}	1.211	1.208	O_{78} - C_{135}	1.207	1.208
O_{18} - C_{25}	1.203	1.208	N_{34} - C_{49}	1.135	1.158	N_{81} - C_{145}	1.137	1.158
S_{14} - C_{30}	1.779	1.782	O_{31} - C_{40}	1.179	1.208	O_{79} - C_{138}	1.208	1.208

Table 2
HOMO – LUMO, Energy Gap (ΔE) and global quantum descriptors of the studied compounds in the gas phase and different solvents.

COMPOUNDS	HOMO eV	LUMO eV	ΔE (eV)	η(eV)	σ(eV)	μ(eV)	χ(eV)	Ω(eV)
A3	-7.0834	-3.5780	3.5053	1.7526	0.2852	-5.3307	5.3307	8.1065
A4	-7.0817	-3.5783	3.5034	1.7517	0.2854	-5.3300	5.3300	8.1088
A5	-7.0825	-3.5791	3.5034	1.7517	0.2854	-5.3308	5.3308	8.1113
WATER								
A3	-6.8915	-3.3687	3.5227	1.7613	0.2838	-5.1301	5.1301	7.4709
A4	-6.8910	-3.3725	3.5184	1.7592	0.2842	-5.1318	5.1317	7.4849
A5	-6.8926	-3.3739	3.5187	1.7593	0.2841	-5.1332	5.1332	7.4887
DMSO								
A3	-6.8953	-3.3728	3.5225	1.7612	0.2838	-5.1341	5.1341	7.4830
A4	-6.8951	-3.3763	3.5187	1.7593	0.2841	-5.1357	5.1357	7.4958
A5	-6.8967	-3.3777	3.5189	1.7594	0.2841	-5.1372	5.1372	7.4996
ETHANOL								
A3	-6.9038	-3.3818	3.5219	1.7609	0.2839	-5.1428	5.1428	7.5095
A4	-6.9032	-3.3842	3.5189	1.7594	0.2841	-5.1437	5.1437	7.5187
A5	-6.9010	-3.3557	3.5453	1.7726	0.2820	-5.1284	5.1283	7.4182
CHLOROFORM								
A3	-6.9565	-3.4351	3.5214	1.7607	0.2839	-5.1958	5.1958	7.6665
A4	-6.9560	-3.4191	3.5369	1.7684	0.2827	-5.1875	5.1875	7.6085
A5	-6.9582	-3.4389	3.5192	1.7596	0.2841	-5.1986	5.1986	7.6793

in the gas phase were 3.5053 eV for A3, 3.5034 eV for A4, and 3.5034 eV for A5. This result shows that the activity of the compounds is in close range, as the softness and hardness values were also in close range with energy differences of -0.0002 eV and 0.0009 eV, respectively. Considering the polar solvents (water, ethanol and DMSO), keen observation revealed substantial changes in the HOMO and LUMO energies which decreased from -6.8910 eV (A4) to -6.8926 eV (A5) and from -3.3725 eV (A4) to -3.3687 eV (A3) for the water medium, from -6.8951 eV (A4) to -6.8967 eV (A5) and from -3.3728 eV (A3) to -3.3777 eV (A5) for the DMSO medium and from -6.9010 eV (A5) to -6.9038 eV (A3) and from -3.3818 eV (A3) to -3.3557 eV (A5) for EtOH medium. The energy gap data shows that the energies of the compounds increased in polar media and were greater for compound A3, which had ΔE values of 3.5227 eV in water, and 3.5225 eV in DMSO, while compound A5 had the highest ΔE in all phases, with a ΔE value of 3.5453 eV in EtOH.

On investigation of the compounds in a non-polar solvent, there was also an increase in the HOMO, LUMO, energy gap and other computed quantum descriptors. The HOMO and LUMO energies ranged from -6.9560 eV (A4) to -6.9582 eV (A5) and from -3.4191 eV (A4) to -3.4389eV (A5), while the highest band gap of 3.5369 eV was observed for compound A4. On observation, the quantum reactivity descriptors showed close differences confirming that the differences in the activities of the compounds are not very conspicuous. In polar solvents, electric charge separation occurs within molecules, leading to the development of an electric dipole moment. On the other hand, non-polar solvents are those in which the charge distribution is evenly spread out in all directions, resembling a spherical symmetry [37]. This principle was applied to assess how different solvents impact a compound's reactivity. Examining the energy gap of the compound across various solvents such as water, DMSO, ethanol, and chloroform (**as presented in** Table 2), our findings reveal noteworthy insights. Notably, the compounds exhibited heightened reactivity in the gas phase, while compound A3 was more stable in water, with an energy gap of 3.5227 eV, compound A4 was more stable in chloroform, with an energy gap of 3.5369 eV, while compound A5 was more stable in EtOH with energy of 3.5453 eV. The energy difference was calculated to be 0.04 eV suggesting that there is a slight or no effect of the solvent on the reactivity and stability of the studied compounds. Figure 2 depicts.

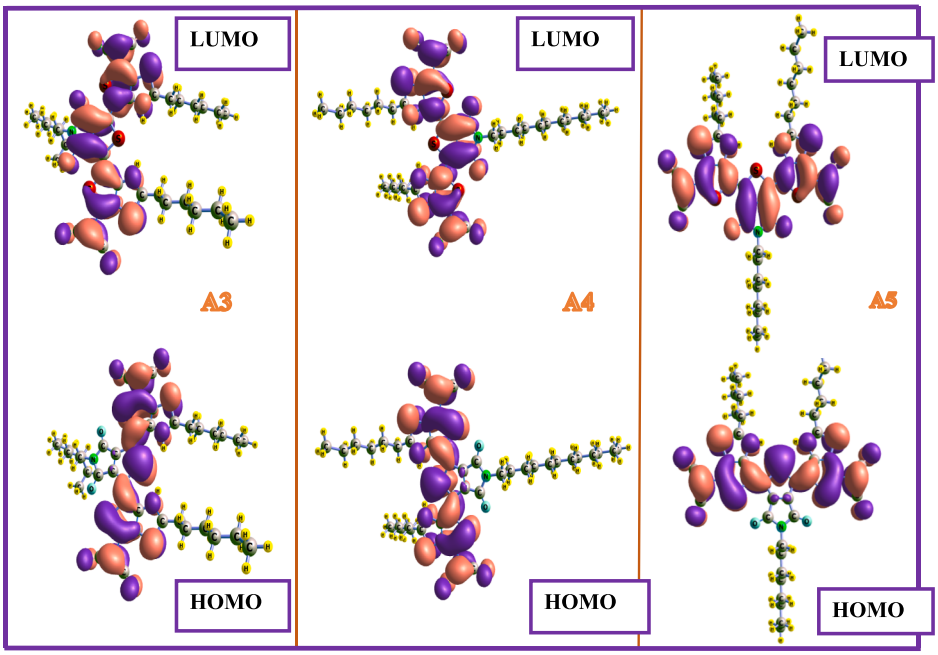

Figure 2. 3-Dimensional maps of the HOMO/LUMO electron distribution of the 2D P-expanded quinoidal terthiophene (2DQTT) compounds labelled A3, A4 and A5.

3.1.2. Natural bond orbital (NBO) analysis

The study of natural bond orbital (NBO) analysis offers a framework for investigating charge transfer and intramolecular bonding within molecular systems. In essence, the stability of donor-acceptor interactions involving unoccupied and occupied NBOs is inherently tied to the delocalization of electron density [38]. It also provides insights into intermolecular and intramolecular charge transfer, as well as the stability relationship between donor and acceptor orbitals [39]. To comprehend the electron distribution in both atomic and molecular orbitals, the concept of bonded orbitals has come into play. These orbitals can be derived from atomic charges and molecular bonds. Photophysical and photorelaxation studies on the other hand, delve into the behavior of molecules when they absorb light and transition to higher energy electronic states [40]. Natural bond analysis comes into play by providing insights into the distribution of electrons and the nature of bonding and interactions within these excited states, offering a deeper understanding of the mechanisms underlying various photophysical phenomena. Additionally, excited states can exhibit high delocalization of electrons, leading to alterations in bonding patterns hence, NBO analysis helps to quantify the extent of delocalization, which is critical for understanding the stability and reactivity of excited states [41]. Previously reported analyses revealed that crucial non-occupied NBOs are antibonding orbitals, and a commonly utilized technique for gauging energy effects is the second-order perturbation energy [42]. For this study, NBO analysis was conducted using the same level of theory as stated earlier, in four solvents (water, dimethyl sulfoxide (DMSO), ethanol and chloroform) to scrutinize each solvent's impact on the compounds of interest and the results are reported in **Table S1** of the supporting information.

Greater stabilization energy indicates more pronounced interactions between donor and acceptor orbitals, potentially arising from enhanced conjugation and robust electron-donating capabilities. Second-order perturbation energies (E^2) highlight the two dominant interactions for the gas phase and each of the solvents (water, DMSO, ethanol, and chloroform). In the gas phase, compound A3 showed backwards transitions from πC_1-$O_9 \rightarrow \sigma^* C_{39}$-$H_{43}$ and πC_1-$O_9 \rightarrow \sigma^* C_{42}$-$H_{47}$ with perturbation energies of 58.73 kcal/mol and 50.44 kcal/mol respectively. Compound A4 showed highest perturbation energies at the forward transition of σC_{24}-$C_{64} \rightarrow \sigma^* C_{65}$-$N_{67}$ and backward transition from πC_{30}-$C_{32} \rightarrow \sigma^* C_{31}$-$C_{69}$ with respective energies of 31.01 kcal/mol and 30.14 kcal/mol respectively. Additionally, compound A5 recorded exhibited the perturbations of 40.03 kcal/mol and 30.60 kcal/mol from the forward and reverse transitions of πC_5-$O_{10} \rightarrow \sigma^* C_{89}$-$H_{92}$ and πC_{30}-$C_{32} \rightarrow \pi^* C_{31}$-$C_{69}$ respectively which shows that compound A3 is more stable in the gas phase, while compound A4 has the stability. Compared with the different solvents, compound A5 demonstrated high perturbation and stability with E^2 values of 170.19 kcal/mol (σC_2-$C_3 \rightarrow \sigma^* C_{15}$-$C_{17}$) in water, 169.02 kcal/mol (σC_2-$C_3 \rightarrow \sigma^* C_{15}$-$C_{17}$) in DMSO, 166.66 kcal/mol (σC_2-$C_3 \rightarrow \sigma^* C_{15}$-$C_{17}$) in EtOH and 154.62 kcal/mol (πC_1-$O_9 \rightarrow \sigma^* C_{15}$-$C_{17}$) in chloroform, and it was more abundant in the water phase. Moreover, compounds A3 and A4 demonstrated the highest stability in water (150.69 kcal/mol and 76.12 kcal/mol respectively). The substantial energy obtained in water might stem from the minimal energy gap between the electron donor and acceptor moieties which are in close proximity with the gas phase. This outcome aligns with the findings from Frontier Molecular Orbital (FMO) analysis, confirming the greater stability of the compounds in water, as observed herein. Moreover, this analysis was applied to assess the influence of solvents on the excited states. Understanding how the solvent environment affects the electronic structure and interactions in the excited state, contributes to the overall photophysical behavior.

3.1.3. Nonlinear optics (NLO) analysis

Nonlinear optics (NLO) has found diverse applications in fields like such as the communication optoelectronic and photonic industries [43]. The interaction between theoreticians and experimentalists has led to the utilization of various methodologies to determine hyper – polarizability and, researchers have used nonlinear optical effects to create new types of lasers, develop optical switches, and study molecular structures and modulators [44]. NLO properties can be correlated with electronic structure characteristics, such as the distribution of electron density, and polarizability and it accurately explain the excited state in a density functional [45]. NLO techniques also provide valuable information about the organization of molecules in a material and their response to intense light [46]. We conducted NLO assessments of the target compounds in four distinct solvents (water, DMSO, ethanol, and chloroform). This analysis aimed to elucidate the dipole moment, static polarizability, and static first hyper - polarizability of the compounds under study. Urea, the initial compound examined for its NLO properties, frequently serves as a reference point for comparison [47]. The first hyper-polarizability, represented as a third-rank tensor, can be described by a 3x3x3 matrix. Employing Kleimann's symmetry, the 27 components of the 3D matrix can be reduced to 10 constituents [48] The polarizability (α) and first order hyper-polarizability (β) are determined by utilizing the **equations 8-10,** as displayed in the methodology section, while the results of the dipole moment, static polarizability, and hyper-polarizability of the compounds (A3, A4, A5) in the gas phase and four solvents are presented in Table 3**.**

These results revealed that compound A3 had the most significant dipole moment in the gas phase and polar solvents (water, DMSO, ethanol) with values of 9.122 D, 12.413 D, 12.339 D and 12.191 D observed for the gas phase, water, DMSO, and ethanol, whereas in chloroform, a non-polar solvent, compound A5 had the highest dipole of 11.103 D. According to previously reported literature, species with narrower energy gaps tend to exhibit elevated static polarizability and hyper-polarizability [49]. This pattern is strongly corroborated by compound A4, which exhibited the lower energy gap in both the gas phase and the polar solvents in the FMO analysis Herein, A4 exhibited the highest static polarizability values of -434.868 a.u, -460.347 a.u, -459.818 a.u, -458.705 a.u and -450.175 a.u corresponding to gas, water, DMSO, ethanol and chloroform respectively and the highest hyper-polarizability of 436.272 a.u in gas phase. Moreover, compound A3 boasts the highest hyper-polarizability of 573.441 a.u, 571.535 a.u, 570.454 a.u, and 536.906 a.u in water, DMSO, EtOH, and chloroform respectively. The static polarizability order among the gas phase and four solvents was as follows: water > DMSO > ethanol > chloroform > gas. The same trend was observed for the hyper-polarizability of the

Table 3
Dipole moment, static polarizability, anisotropy and hyperpolarizability of the studied compounds were calculated for different solvents.

SYSTEMS	Dipole moment (μ)	Static Polarizability (α total)	Anisotropy of the Polarizability (Δα)	Static Hyperpolarizability
GAS				
A3	9.122	-406.727	132.95	319.068
A4	8.612	-434.868	263.97	436.272
A5	8.638	-413.689	247.18	434.913
WATER				
A3	12.413	-443.369	331.17	573.441
A4	12.339	-460.347	360.64	482.959
A5	12.407	-441.866	340.35	563.741
DMSO				
A3	12.339	-442.783	329.33	571.535
A4	12.267	-459.818	358.78	483.102
A5	12.335	-441.301	338.60	562.259
ETHANOL				
A3	12.191	-441.573	326.98	570.454
A4	12.117	-458.705	354.88	483.387
A5	11.714	-437.890	323.03	538.707
CHLOROFORM				
A3	11.088	-433.066	177.15	536.906
A4	10.828	-450.175	177.15	482.292
A5	11.103	-431.518	177.15	525.459

compounds. The substantial hyper-polarizability in water and DMSO might stem from its charge transfer properties, as the electron cloud transits from a donor to an acceptor region. Additionally, the pronounced anisotropy values observed for compound A4 in all studied solvents indicate that the physical properties of the compounds are more likely to change in these solvents, while a high value is noted in the gas phase for compound A5. These findings collectively suggest that the studied compounds are notably polarizable across all solvents, especially compound A4 which showed polarization efficacy in all the solvents, indicating its potential utility in diverse fields that require nonlinear activity.

3.2. Excited state analysis

3.2.1. UV/Vis excitation analysis

UV analysis is viewed as a cornerstone when considering photophysical and photorelaxation studies because it allows researchers to probe the electronic transitions, absorption behavior, and photochemical processes during electronic excitation [50]. A dye with high efficiency must possess a strong and broad absorption band over visible light (400–800 nm). The information obtained through UV analysis is essential for revealing the intricate details of how molecules interact with light and how they undergo photophysical and photochemical transformations [51]. Monitoring the changes in UV absorption during such reactions can provide insights into reaction kinetics, reaction mechanisms, and photo-induced processes. Additionally, UV analysis can reveal how solvation affects the absorption behavior of organic compounds and molecules [52]. Different solvents can lead to shifts in absorption bands due to changes in the molecular environment and interactions between the solvent and solute. Herein, we introduce four solvents (polar and non-polar) to study the photophysical activities and photorelaxation responses of 2D p-expanded quinoidal terthiophene (2DQTT) compounds labelled A3, A4, and A5, which have been suggested to have light emitting properties that can improve the optoelectronics industry, as well as DSSC, which is a revolutionary technology that leverages organic materials to create efficient, vibrant, and flexible light sources [53]. This study considered various indices used to assess the excited state of compounds in UV analysis, including the excitation energy, wavelength, oscillator strength, the accompanied electron major contributors (MCs) and transitions observed from the ground state to the second excited state with the aim of revealing crucial insights into how solvation affects the studied compounds. To achieve this, the Gaussian 09 solvation model, also known as the conductor-like polarizable continuum (CPCM) model, was utilized [54]. The electronic properties, such as the oscillator strength (F), wavelength (λmax), and excitation energy (E), are presented in Table 4. From the depicted results in Table 4, the gas phase which represents as the point of reference and comparison, showed an electronic transition from HOMO to LUMO from H→L and H→L+1 for compounds A3, A4, and A5 for the first and second excitation states respectively with the highest absorption spectrum occurring at the first excitation state corresponding to a wavelength of 635.35 nm for all compounds with the major contribution and oscillator strength presented at 97.142% and 1.2765 for A4 and A5, respectively, whereas A3 had the greatest contribution and oscillator strength of 98.564% and 1.2672, respectively. Going forward, it is important to summit that in UV analysis, the parameters are explained following keen principles. A good system has a low energy, long wavelength and high oscillator strength [55]. Considering the influence of the different solvents, we observed that compound A3 had the longest absorption wavelength of 785.32 nm in water with an oscillator strength of 2.0136 and the highest contribution of 97.014% with a solvent influence and contribution trend of water > DMOS (782.32) > ethanol (768.47) > chloroform (731.43) > gas. Compound A4 was also observed to have the longest absorption wavelength of 787.13 nm in water with an oscillator

Table 4
UV – vis excitation energies, transitions, percentage contributions and oscillator strengths for the studied compounds in different solvents.

COMPOUNDS	Excitation Type	Energy (eV)	ʎ (nm)	OscillatorStrength	MC (%)	Transition (f)
GAS						
A3	S0→S1	1.9514	635.35	1.2672	98.564	H→L
	S0→S2	3.1338	395.64	0.0081	32.681	H→L+1
A4	S0→S1	1.9515	635.34	1.2745	97.142	H→L
	S0→S2	3.1329	395.75	0.0083	65.290	H→L+1
A5	S0→S1	1.9513	635.38	1.2765	97.142	H→L
	S0→S2	3.1328	395.76	0.0083	65.343	H→L+1
WATER						
A3	S0→S1	1.5788	785.32	2.0136	97.014	H→L
	S0→S2	2.9133	425.58	0.0593	70.081	H→L+1
A4	S0→S1	1.5751	787.13	2.0119	97.025	H→L
	S0→S2	2.9115	425.84	0.0581	70.313	H→L1
A5	S0→S1	1.5758	786.78	2.0143	97.022	H→L
	S0→S2	2.9122	425.74	0.0588	70.230	H→L1
DMSO						
A3	S0→S1	1.5848	782.32	2.0028	97.014	H→L
	S0→S2	2.9194	424.69	0.0588	70.513	H→L1
A4	S0→S1	1.5812	784.10	2.0014	70.724	H→L
	S0→S2	2.9176	424.95	0.0577	76.899	H→L1
A5	S0→S1	1.5819	783.74	2.0038	97.022	H→L
	S0→S2	2.9183	424.85	0.0583	70.641	H→L1
ETHANOL						
A3	S0→S1	1.6134	768.47	1.9640	97.081	H→L
	S0→S2	2.9732	417.00	0.0446	67.822	H→L1
A4	S0→S1	1.6112	769.51	1.9642	97.087	H→L
	S0→S2	2.9720	417.18	0.0450	68.106	H→L1
A5	S0→S1	1.6118	769.23	1.9647	75.906	H→L
	S0→S2	2.9725	417.11	0.0452	68.214	H→L1
CHLOROFORM						
A3	S0→S1	1.6951	731.43	1.7969	65.018	H→L
	S0→S2	3.0231	410.12	0.0508	81.069	H→L1
A4	S0→S1	1.7126	723.97	1.7784	97.142	H→L
	S0→S2	3.0776	402.86	0.0401	77.765	H→L1
A5	S0→S1	1.6933	732.19	1.8031	97.048	H→L
	S0→S2	3.0223	410.23	0.0520	81.149	H→L1

strength of 2.0119 and the highest contribution of 97.025%, with a solvent trend of water > DMOS (784.10) > ethanol (769.51) > chloroform (723.97) > gas. Additionally, for in compound A5, we observed the same trend was the case which is as follows; water (786.78) > DMOS (783.74) > ethanol (769.23) > chloroform (732.19) > gas (635.38). This analysis revealed that water as a media of optimization has a strong effect on enhancing the photophysical and photorelaxation of the compounds which could be due to its high polarity due to its strong hydrogen bonding capabilities and dielectric constant of ~78.5 which reflects the degree of polarization that a material experiences in response to an applied electric field. The dielectric constant of a material can provides insights into its ability to shield and interact with electric charges [56]. Therefore, the high degree of excitation of the compounds was evident in their high absorption wavelengths which were observed as follows, A4 > A5 > A3. These results show that the compounds are proficient materials for photophysical applications, and the results clearly agree with the nonlinear optics and natural perturbation energy analysis of the compounds. It is also important to note that a higher absorption wavelength was obtained at the first excitation state, while moving to the second, the λ_{max} decreased with increasing energy.

3.2.2. Hole-electron analysis

Photophysical processes often involve charge transfer between different parts of an organic compound or between molecules. Hole-electron analysis (HEA) helps identify the regions that act as electron donors and acceptors, providing insights into the charge transfer mechanisms that drive excited-state behavior [57]. When an electron is excited to a higher energy level, it leaves behind an empty state in the valence band called hole. Hole electron analysis helps us to determine the energy levels and distribution of electron densities which also helps determine the material's electrical and optical properties [58]. To investigate the influence of solvents on the photophysical and photorelaxation properties of 2D p-expanded quinoidal terthiophene (2DQTT) compounds, hole electron analysis was employed to provide a deeper understanding of the electronic structure, charge distribution, and excited-state dynamics of molecules undergoing photoexcitation and relaxation [59]. This analysis helps elucidate the movement of charge carriers (holes and electrons) within different compounds and also reveals how solvation affects charge localization and charge transfer processes. The data in Table 5 are crucial for understanding the electronic properties, charge distribution, and behavior of the studied compounds during photoexcitation and relaxation. The compounds showed similar exciton binding energies which were highest in the gas phase. This is the energy required to dissociate an exciton (electron-hole pair) created during the excitation phase and measures how tightly the electron and hole are bound. All of these results were lower in water which therefore suggests that phonons absorbed by compounds A3, A4, and A5 in water medial have a greater possibility of generating excitons than those in the other phase. The t index measures how far apart the hole and electron are from each other in the charge transfer (CT) direction [60]. It is calculated by taking the numerical difference between the H value and the D value in the CT direction as given in **equation 11**.

$$tindex = Dindex - HCT \quad (11)$$

The t index values which are less than zero for the compounds in both gas and solvent media, indicate there is no significant separation between the hole and electron due to charge transfer. By employing **equation 12**, the distance between the hole and an electron on average density which is explained by the H index, is given. The H_{CT} measures how the strains are spread out in the XYZ direction.

$$Hindex = (|\boldsymbol{\sigma ele}| + |\boldsymbol{\sigma} hole|)/2 \quad (12)$$

One way to gauge this could involve measuring the gap between the center of the hole and the center of the electron, both in their respective directions. This is illustrated by **equation 13**, where the complete measurement of this charge transfer length is denoted as the D index [61].

$$Dindex = |D| \equiv \sqrt{(D_x)^2 + (D_Y)^2 + (Dz)^2} \quad (13)$$

A smaller hole delocalization index (HDI) or electron delocalization index (EDI) indicates that the hole (or electron) is spread out more widely across the system. In simpler terms, the charge is evenly distributed over a larger area [62]. Both the HDI and EDI are valuable for measuring how broadly the charge is distributed in space and are mathematically calculated using **equations 14 and 15,** and it was observed that the compounds in all phases had small HDIs and EDIs which means that electrons are widely delocalized by the compounds upon excitation from the ground state to the first excitation state. The hole delocalization index (HDI) and electron delocalization index (EDI) are defined as follows:

$$EDI = 100x\sqrt{\int [\rho^{ele}(r)]^2 dr} \quad (14)$$

$$HDI = 100x\sqrt{\int [\rho^{hole}(r)]^2 dr} \quad (15)$$

Table 5
Hole – electron analysis of the first excited parameters of 2D P-expanded quinoidal terthiophene (2DQTT) compounds labelled A3, A4 and A5 in gas and solvent media.

COMPOUNDS	Excitation	t-index (Å)	H-index (Å)	HDI	EDI	D-index(Å)	Sr index (a.u)	Exciton binding energy (eV)
GAS								
A3	S0-S1	-1.151	4.927	5.18	5.34	0.700	0.690	1.951
A4	S0-S1	-1.065	4.945	5.31	5.20	0.582	0.703	1.952
A5	S0-S1	-1.108	4.932	6.34	5.25	0.597	0.703	1.951
WATER								
A3	S0-S1	-1.269	4.969	5.14	5.27	0.578	0.705	1.579
A4	S0-S1	-1.064	4.955	5.52	5.20	0.588	0.703	1.575
A5	S0-S1	-1.183	4.975	5.22	5.20	0.571	0.707	1.576
DMOS								
A3	S0-S1	-1.269	4.969	5.14	5.27	0.579	0.705	1.585
A4	S0-S1	-1.063	4.953	5.62	5.20	0.589	0.703	1.581
A5	S0-S1	-1.181	4.975	5.21	5.20	0.571	0.707	1.582
ETOH								
A3	S0-S1	-1.219	4.943	5.16	5.22	0.599	0.701	1.613
A4	S0-S1	-1.065	4.945	5.31	5.20	0.582	0.703	1.611
A5	S0-S1	-1.108	4.932	6.33	5.25	0.597	0.702	1.612
CHLOROFORM								
A3	S0-S1	-2.261	5.117	3.64	3.57	0.208	0.957	1.695
A4	S0-S1	-1.259	4.909	5.87	5.24	0.611	0.703	1.713
A5	S0-S1	-1.129	4.938	6.23	5.21	0.595	0.700	1.693

Meanwhile, the degree of charge transfer (Sr) in the excited state, given in atomic units, shows a close range of disparities in the various phases ranging from 0.690 a.u in gas to 0.957 a.u in chloroform for compound A3. In fields such as organic electronics and photovoltaics, understanding hole and electron movement is crucial for designing efficient charge transport materials, and their distribution helps predict and explain the outcome of photochemical reactions by tracking the movement of holes and electrons, which can help researchers gain insights into the timescales and pathways of excited-state relaxation [63].

3.3. Relaxation dynamics

3.3.1. Geometry optimization

The geometry of the molecule, which includes the arrangement of its atoms, bond lengths and angles, plays a crucial role in determining how quickly and through which pathways photorelaxation occurs. Photorelaxation described earlier refers to the process by which a photo excited molecule returns to its ground state after absorbing light energy, and it is important to note that solvent interactions can modify the molecule's geometry upon excitation [64]. This can affect relaxation dynamics by altering the potential energy surfaces and relaxation pathways. The distance between two nucleic atoms in the 2D P-expanded quinoidal terthiophene (2DQTT) compounds was investigated for relaxation while comparing with experimental bond distances at points of heteroatom bonding. The computed results are depicted in Table 6 and the results show that in compound A3, the theoretical bond length varied, showing alternating increases and decreases in bond distances. A decrease in the number of bonds was observed for S_{13} - C_{29} (1.765 Å), S_{16} - C_{41} (1.761 Å) and S_{14} - C_{30} (1.761 Å) compared with the experimental values of 1.766 Å, 1.771 Å and 1.779 Å, respectively, corresponding to the different labels. In compound A4, an alternating bond length increase and decrease was observed, which was also observed during the excitation structural analysis with shorter theoretical bond lengths observed for S_{29} - C_{54} (1.743Å), and N_{32} - C_{37} (1.395Å) with corresponding experimental bond lengths of 1.747 Å and 1.396 Å respectively. Considering compound A5, short bond lengths were observed in S_{74} - C_{140}, S_{73} - C_{149}, and N_{80} - C_{138} with experimental and theoretical bond lengths of 1.774 Å, 1.770 Å, 1.397 Å and 1.761 Å, 1.765 Å and 1.395 Å respectively. According to Wang et al [65], a shorter bond length leads to the formation of strong bonds, and the molecule becomes more stable, while instability occurs for longer bonds. Moreover, the bond distances between atoms of compounds are important for charge transfer processes between donor and acceptor groups in photovoltaics and solar cells, as ICT is more favoured at points of shorter bonds [66]. In our study, we noticed that the relaxation of the compounds led to changes in the bonds and structural conformation of the 2D P-expanded quinoidal terthiophene (2DQTT) compounds as the compounds de-excite back to a lower energy level which caused a change in structural bonding (Stokes shift) in the heteroatoms.Table 7.

3.3.2. Hole-electron relaxation

Hole analysis of photo relaxation was performed using a density functional approach, which helps us understand how electrons move within a molecule after it absorbs light (undergoes photoexcitation). Upon relaxation, photoexcited molecule adjusts its electronic configuration to reach a stable state. This can involve electron movement in response to the hole that was left behind, and investigating the movement of this hole helps us understand how the organic compound's electrons rearrange themselves to accommodate the energy absorbed from the light which further helps us understand how the molecule stabilizes after absorbing light [67]. The relaxation hole analysis showed significant changes in fluorescence compared to that observed after the absorption of the 2D P-expanded quinoidal terthiophene (2DQTT) compounds. The t- index that describes charge transfer indicates that the charges were < 0 for all the compounds and in all phases which suggests a minute amount of CT on relaxation of the molecules. This observation in comparison with the excitation analysis revealed greater charge transfer throughout all phases during photophysical excitation. The D-index was quantitatively observed to be very low for relaxations ranging from 0.460 Å in DMSO phase to 0.566 Å in the gas phase, which indicates that the distance between the centroids of the holes and electrons is relatively close, moreover, although the H-index is relatively high, we can assert that the compounds are in local excited states. However, we noticed that the overlap of holes and electrons is very large due to the high Sr values observed ranging from 0.744 a.u in gas for A3 to 0.796 a.u in ethanol for A3 which means that only a small degree of electron migration is observed herein.

3.4. Photovoltaic analysis

Photophysical and photo-relaxation studies generally focus on understanding the various processes that occur when light interacts with materials, often including relaxation mechanisms that follow photoexcitation. The photovoltaic characteristics include factors such as the injection's negative free energy (ΔG^{inject}), the light harvesting efficiency (LHE), the oxidation energy of the 2DQTTs compound in its ground state (E^{2DQTTs}), the oxidation energy of the 2DQTTs in its excited state (E^{2DQTTs}), and the open circuit photovoltage (Voc). The outcomes of these parameters are illustrated in the findings and reported in Table 8. The open circuit photovoltage serves as a tool for assessing the power conversion efficiency (η) in DSSCs [68]. Typically, electron transfer occurs from the LUMO of dye molecules to the semiconductor conduction band. Consequently, if the E_{LUMO} is elevated, the Voc will also be increase, leading to an enhanced driving force for regeneration, which can in turn enhance η_{reg} [69]. In DFT photovoltaic analysis, the open circuit voltage (Voc) is the energy difference between the redox potential of the electrolyte's redox couple I^-/I_3^- and the quasi-Fermi level located in the semiconductor's conduction band (TiO_2) [70]. It is expressed mathematically as follows

$$Voc = \frac{E_{CB} + \Delta CB}{q} + \frac{KT}{q} + ln\frac{n_C}{N_{CB}} - \frac{E_{Redox}}{q} \quad 15$$

Table 6
Theoretical and experimental bond length analysis of 2D P-expanded quinoidal terthiophene (2DQTT) dye compounds for relaxation, studied at the CAM-B3LYP/6-31+G (d,p) level of theory.

COMPOUNDS	A3			A4			A5	
	BOND DISTANCES (Å)			BOND DISTANCES (Å)			BOND DISTANCES (Å)	
BOND LABEL	Experimental	Theoretical	BOND LABEL	Experimental	Theoretical	BOND LABEL	Experimental	Theoretical
S_{13} - C_{29}	1.766	1.765	S_{27} - C_{53}	1.748	1.761	S_{75} - C_{142}	1.706	1.725
S_{16} - C_{41}	1.771	1.761	S_{29} - C_{54}	1.747	1.743	S_{74} - C_{140}	1.774	1.761
N_{20} - C_{25}	1.391	1.396	S_{25} - C_{41}	1.758	1.765	S_{73} - C_{149}	1.770	1.765
S_{17} - C_{43}	1.708	1.725	N_{32} - C_{37}	1.396	1.395	N_{80} - C_{138}	1.397	1.395
S_{15} - C_{32}	1.713	1.725	O_{30} - C_{37}	1.211	1.217	O_{78} - C_{135}	1.207	1.217
O_{18} - C_{25}	1.203	1.217	N_{34} - C_{49}	1.135	1.159	N_{81} - C_{145}	1.137	1.159
S_{14} - C_{30}	1.779	1.761	O_{31} - C_{40}	1.179	1.217	O_{79} - C_{138}	1.208	1.217

Table 7
Hole - electron analysis of the first excited state parameters of the 2D P-expanded quinoidal terthiophene (2DQTT) compounds on relaxation labelled A3, A4 and A5 in gas and solvent media.

COMPOUNDS	Excitation	t-index (Å)	H-index (Å)	HDI	EDI	D-index(Å)	Sr index (a.u)	Exciton binding energy (eV)
GAS								
A3	S0-S1	-1.306	5.092	4.96	5.07	0.566	0.744	1.643
A4	S0-S1	-1.139	5.093	5.06	5.07	0.552	0.749	1.642
A5	S0-S1	-1.187	5.097	4.98	5.13	0.563	0.748	1.642
WATER								
A3	S0-S1	-1.326	5.118	5.45	5.16	0.512	0.758	1.579
A4	S0-S1	-1.186	5.117	5.22	5.06	0.505	0.754	1.575
A5	S0-S1	-1.246	5.132	4.95	5.04	0.514	0.751	1.576
DMSO								
A3	S0-S1	-1.272	5.187	5.08	5.16	0.472	0.796	1.082
A4	S0-S1	-1.522	5.188	5.10	5.07	0.460	0.789	1.097
A5	S0-S1	-1.191	5.186	5.07	5.15	0.470	0.794	1.080
ETHANOL								
A3	S0-S1	-1.364	5.120	5.07	5.15	0.513	0.752	1.613
A4	S0-S1	-1.174	5.112	5.19	5.13	0.517	0.754	1.611
A5	S0-S1	-1.211	5.101	5.75	5.13	0.520	0.753	1.612
CHLOROFORM								
A3	S0-S1	-1.293	5.169	5.07	5.13	0.494	0.786	1.269
A4	S0-S1	-1.233	5.164	5.06	5.14	0.490	0.778	1.281
A5	S0-S1	-1.266	5.159	5.36	5.23	0.491	0.785	1.272

Table 8
Electron injection-related properties of various 2D P-expanded quinoidal terthiophene (2DQTT) dye compounds labelled A3, A4 and A5 in gas and solvent media.

SOLVENT	COMPOUND	Voc	*F*	LHE	λmax	ΔG_{inject}	ΔG_{reg}	ΔG_{CR}
GAS	A3	3.868	1.275	4.668	635.35	3.868	-17.85	7.118
	A4	3.868	1.274	4.668	635.34	3.868	-17.81	7.118
	A5	3.868	1.276	4.668	635.38	3.868	-17.90	7.118
WATER	A3	3.876	2.013	4.676	785.32	3.876	-89.33	7.126
	A4	3.876	2.017	4.676	787.13	3.876	-101.2	7.126
	A5	3.876	2.014	4.676	786.78	3.876	-102.2	7.126
DMOS	A3	3.873	2.002	4.676	782.32	3.873	-99.65	7.126
	A4	3.875	2.010	4.675	784.10	3.875	-99.95	7.125
	A5	3.875	2.003	4.675	783.74	3.875	-99.88	7.125
ETHANOL	A3	3.876	1.964	4.676	768.47	3.876	-91.04	7.126
	A4	3.876	1.964	4.676	769.51	3.876	-91.09	7.126
	A5	3.876	1.945	4.676	769.23	3.876	-91.07	7.126
CHLOROFORM	A3	3.873	1.796	4.673	731.43	3.873	-61.65	7.123
	A4	3.874	1.778	4.674	723.97	3.874	-59.03	7.124
	A5	3.873	1.803	4.673	732.19	3.873	-62.55	7.123

where, E_{CB} represents the conduction band edge of TiO_2, q represents the elementary charge unit, T denotes the absolute temperature, k represents the Boltzmann constant, n_C corresponds to the number of electrons in the conduction band, and N_{CB} signifies the density of available states within the conduction band. Additionally, E_{redox} designates the redox potential of the electrolyte. The parameter ΔCB signifies the shift of the conduction band when the dyes are adsorbed. This relationship is expressed mathematically as follows:

$$\Delta CB = \frac{q\mu_{normal}\gamma}{\varepsilon_0\varepsilon} \quad 16$$

In this context, μ_{normal} represents the dipole moment of an individual dye molecule, oriented perpendicular to the surface of TiO_2. The variable γ signifies the concentration of the dye on the surface. Additionally, the constants ε_0 and ε correspond to the vacuum permittivity and dielectric permittivity, respectively. The estimation of Voc can also be approximated using the difference between E_{LUMO} and E_{CB}. This approach is chosen because the dyes under study do not exist in an adsorbed state on TiO_2 [71]. Consequently, the calculations of n_c and N_{CB} serve this purpose. Meanwhile, J_{SC}, the short-circuit current density, can be mathematically described as;

$$J_{SC} = \int LHE(\lambda)\acute{E}_{\lambda,inject}\eta_{inject}d\lambda \quad 17$$

where, LHE (λ) signifies the light-harvesting efficiency at the wavelength of maximum absorption, ϕ_{inject} represents the efficiency of electron injection, and $\eta_{collect}$ represents the efficiency of charge collection. Achieving a higher J_{SC} requires maximizing both LHE and ϕ_{inject} which should be high. The mathematical representation of LHE is as follows;

$$LHE = 1 - 10^{-f} \quad 18$$

In this equation, *f* represents the oscillator strength of the dye corresponding to the maximum absorption wavelength λ_{max}.

ϕ_{inject} is connected to the thermodynamic driving force ΔG_{inject} for electron injection from the dye's excited states to the conductive band of TiO_2. ΔG_{inject} is mathematically represented as;

$$\Delta G_{inject} = E^{dye^*} - E_{CB}^{TiO_2} \approx E^{dye} + \Delta E - E_{CB}^{TiO_2} \quad 19$$

Here, E^{dye^*} denotes the redox potential of the oxidized dye in the excited state, E^{dye} is the redox potential of the oxidized dye in the ground state, ΔE is the lowest vertical excitation energy, and $E_{CB}^{TiO_2}$ signifies the quasi-Fermi energy level of the TiO_2 conduction band.

ΔG_{reg} (the driving force energy for dye regeneration) is mathematically represented as;

$$\Delta G_{reg} = \mu(I^-/I_3^-) - E^{dye} \quad 20$$

According to a previously reported article, an oxidized dye with a

ΔG_{inject} value exceeding 0.20 eV indicates efficient electron injection [72]. To ascertain J_{SC} which is the maximum current that flows through the solar cell when its terminals are short-circuited (i.e., the voltage across the terminals is zero) and the overall conversion efficiency (μ), Table 8 presents the calculated values of Voc, f, LHE, λmax, ΔG_{inject}, ΔGreg, and ΔGcr across the four different solvents, alongside wavelength changes. **Equation 15** highlights that a dye with a narrower energy band gap facilitates a redshifted absorption spectrum, generating more electrons (higher n_C) and thereby enhancing the Voc efficiency. For the dye compounds labelled A3, A4, and A5 herein, we observed that the open circuit photovoltage (Voc) values ranged from 3.868 eV in gas phase to 3.876 eV in water and ethanol which means that there is a high driving force for regeneration of the dye compounds in the solvents. Notably, for the ΔG_{reg} calculations, it is important to mention that an E_{CB} of approximately 4.00 eV is applied to the TiO_2 semiconductor. ΔG_{reg} is the free energy difference between the electrolyte and the HOMO of the dye molecules. This signifies the ability of the dye to get reduced by the electrolyte to be used in the DSSC [70]. ΔG_{reg} has negative values for the various dye compounds and was greater in water media, with values of -89.33 eV, -102.2 eV, and -101.2 eV for compounds A3, A4, and A5 respectively which suggests that the electrolyte's redox level is situated below the ground states of the chosen dyes, leading to a reduction in electron recombination.

Across all solvents, ΔG_{inject} consistently surpasses 0.2 eV, ensuring efficient electron injection for all dyes in the four solvents including the gas phase. However, dye compound A4 exhibited the highest ΔG_{inject} values in all phases, showing an electron injection magnitude range of water > ethanol > DMSO > chloroform > gas, indicating superior electron injection of dye compound A4. Additionally, the outcomes presented in Table 8 reveal that, among the studied dyes across the five phases, except in gas and chloroform, dye A4 exhibited the highest f values, although in these values were in close to those of other dye compounds. Nevertheless, light harvesting efficiency (LHE) values further indicate the fact that the dye compounds better absorb and efficiently respond to light in water media which is evident from the high LHE of 4.676 eV observed in the water phase for the dye compounds, indicating greater stability of the dyes in water. To accurately predict the short-circuit current density of a dye molecule, it is imperative to enhance both the light harvesting efficiency (LHE) and electro-injection efficiency [74]. The LHE factor is intricately linked to the oscillator strength, and hence, it can be concluded in this study that 2D P-expanded quinoidal terthiophene (2DQTT) compounds can efficiently relax to a semiconductor, especially under the influence of water, thereby providing great fluorescence.

4. Conclusions

2D P-expanded quinoidal terthiophene (2DQTT) dye compounds were theoretically studied using first principle density functional theory at the CAM-B3LYP/6-31+G (d,p) method to investigate the ground state electronic structural properties, reactivity, and bonding nature involved in photophysical and photo relaxation phenomena, while the excited state molecular properties, and hole electron analysis along with the photovoltaic application of the reactive 2DQTT dye compounds were extensively studied using time-dependent density functional theory (TD-DFT) by imploring the CAM-B3LYP method with the 6-31+G(d,p) basis set. The investigation revealed that solvation plays a pivotal role in modulating the electronic and structural properties of 2DQTTs, exerting a pronounced influence on their excited-state behavior. The observed shifts in absorption and emission spectra, along with alterations in the fluorescence lifetimes, point towards the strong interactions between the solvents and the molecular framework of 2DQTTs especially in water acqeous media. The findings reveal that the HOMO and LUMO levels of all the investigated dye compounds are situated within the I^-/I_3^- electrolyte which is necessary to enable charge regeneration. It is also observed that in all the solvents ΔG_{inject} is greater than 0.2 eV. Therefore, all the dyes in the five phases provide efficient electron injection and light harvesting efficiency (LHE) properties which are more conspicuous aqueous media, especially for compound A4. It can be clearly seen that the solvent influences the photophysical processes, which was evident in the variations in the maximum wavelength, energy and oscillator strength observed in all phases, which were greater in the water medium in the first excited state of the compounds. Photo relaxation also showed that upon florescence, the compounds were stable with little or no deviation. Hence, all three dye compounds of 2D P-expanded quinoidal terthiophene (2DQTTs) are good for optoelectronics and DSSC applications. This information is crucial for designing materials that minimize charge carrier recombination and enhance charge transport, leading to higher solar cell efficiency and contributing to advancements in both fundamental understanding and practical applications in the field of materials science and beyond.

CRediT authorship contribution statement

Thomas O. Magu: . **Terkumbur E. Gber:** Writing – review & editing, Writing – original draft, Visualization, Validation. **Rasaq A. Adams:** . **MaryAnn A. Odume:** . **Sunday S. Ikiensikimama:** Visualization, Validation, Investigation.

Declaration of competing interest

The authors declare that they have no known competing financial interests or personal relationships that could have appeared to influence the work reported in this paper.

Data availability

No data was used for the research described in the article.

Acknowledgements

The authors are thankful to all computational Chemistry open-source developers and also for the support provided by the Regional Scholarship and Innovation Fund (RSIF) under the Partnership for Skills in Applied Sciences, Engineering, and Technologies (PASET) Initiative. The are also grateful to the International Centre of Insect Physiology and Ecology (ICIPE) for managing the RSIF fund.

Appendix A. Supplementary data

Supplementary data to this article can be found online at https://doi.org/10.1016/j.comptc.2024.114554.

References

[1] Z.X. Chen, Y. Li, F. Huang, Persistent and stable organic radicals: Design, synthesis, and applications, Chem 7 (2) (2021) 288–332.
[2] P.M. Beaujuge, J.R. Reynolds, Color control in π-conjugated organic polymers for use in electrochromic devices, Chem. Rev. 110 (1) (2010) 268–320.
[3] J. Casado, Para-quinodimethanes: a unified review of the quinoidal-versus-aromatic competition and its implications, Physical Organic Chemistry of Quinodimethanes (2018) 209–248.
[4] Vazquez, R. (2019). Characterizing the Excited State Dynamics of Organic Materials for Efficient Energy Conversion: from Current to Photons and Vice-Versa (Doctoral dissertation).
[5] A.K. Chauhan, P. Jha, D.K. Aswal, J.V. Yakhmi, Organic devices: fabrication, applications, and challenges, J. Electron. Mater. (2022) 1–39.
[6] T.M. Brown, F. De Rossi, F. Di Giacomo, G. Mincuzzi, V. Zardetto, A. Reale, A. Di Carlo, Progress in flexible dye solar cell materials, processes and devices, J. Mater. Chem. A 2 (28) (2014) 10788–10817.
[7] S. Arslancan, L. Martínez-Fernández, I. Corral, Photophysics and photochemistry of canonical nucleobases' thioanalogs: From quantum mechanical studies to time resolved experiments, Molecules 22 (6) (2017) 998.
[8] P.T. Chou, Y. Chi, M.W. Chung, C.C. Lin, Harvesting luminescence via harnessing the photophysical properties of transition metal complexes, Coord. Chem. Rev. 255 (21–22) (2011) 2653–2665.

[9] L. Mencaroni, A. Cesaretti, G. Consiglio, F. Elisei, C.G. Fortuna, A. Spalletti, Photobehavior of an Acidochromic Dinitrophenyl-Hydrazinylidene Derivative: A Case of Total Internal Conversion, Photochem 2 (4) (2022) 849–865.

[10] M.J. Limo, A. Sola-Rabada, E. Boix, V. Thota, Z.C. Westcott, V. Puddu, C.C. Perry, Interactions between metal oxides and biomolecules: from fundamental understanding to applications, Chem. Rev. 118 (22) (2018) 11118–11193.

[11] M.A. Rohman, P. Baruah, S.O. Yesylevskyy, S. Mitra, Specific solvent effect on the photophysical behavior of substituted chromones: A combined fluorescence, DFT and MD study, Chem. Phys. 517 (2019) 67–79.

[12] S. Nath, B. Bhattacharya, U. Sarkar, T.S. Singh, Solvent Effects on the Photophysical Properties of a Donor–acceptor Based Schiff Base, J. Fluoresc. 32 (4) (2022) 1321–1336.

[13] Mangalum, A. (2011). CONJUGATED POLYMERS AND INTER-CHROMOPHORE INTERACTIONS: SYNTHESIS, PHOTOPHYSICAL CHARACTERIZATION AND APPLICATION.

[14] F. Zhang, C.A. Di, Exploring thermoelectric materials from high mobility organic semiconductors, Chem. Mater. 32 (7) (2020) 2688–2702.

[15] C. Zhang, X. Zhu, Thieno [3, 4-b] thiophene-based novel small-molecule optoelectronic materials, Acc. Chem. Res. 50 (6) (2017) 1342–1350.

[16] C. Zhang, Y. Zang, F. Zhang, Y. Diao, C.R. McNeill, C.A. Di, D. Zhu, Pursuing High-Mobility n-Type Organic Semiconductors by Combination of "Molecule-Framework" and "Side-Chain" Engineering, Adv. Mater. 28 (38) (2016) 8456–8462.

[17] Q. Fan, L. Li, H. Xue, H. Zhou, L. Zhao, J. Liu, J. Wang, Precise control over kinetics of molecular assembly: production of particles with tunable sizes and crystalline forms, Angew. Chem. 132 (35) (2020) 15253–15258.

[18] R. Dennington., T.A. Keith., & J. M. Millam., GaussView 6.0. 16. Semichem Inc.: Shawnee Mission, KS, USA. HyperChem, T. (2001). HyperChem 8.07, HyperChem Professional Program. Gainesville, Hypercube. (2016).

[19] Frisch, A. (2009). gaussian 09W Reference. *Wallingford, USA, 25p, 470*.

[20] X. Dai, Q. Meng, F. Zhang, Y. Zou, C.A. Di, D. Zhu, Electronic structure engineering in organic thermoelectric materials, Journal of Energy Chemistry 62 (2021) 204–219.

[21] K.P. Babu, S. Manimegalai, Investigations of absorption and magnetic resonance spectroscopies, molecular docking studies and quantum chemical calculations of 3-Hydroxy-4-methoxybenzaldehyde, Indian Journal of Pure & Applied Physics (IJPAP) 60 (1) (2022) 49–58.

[22] S. Sevvanthi, S. Muthu, M. Raja, S. Aayisha, S. Janani, PES, molecular structure, spectroscopic (FT-IR, FT-Raman), electronic (UV-Vis, HOMO-LUMO), quantum chemical and biological (docking) studies on a potent membrane permeable inhibitor: dibenzoxepine derivative, Heliyon 6 (8) (2020).

[23] V.L. Chandraboss, B. Karthikeyan, S. Senthilvelan, Experimental and first-principles investigation of the adsorption and entrapping of guanine with SiO 2 clusters of sol–gel silicate material for understanding DNA photodamage, PCCP 17 (18) (2015) 12100–12114.

[24] F. Weinhold, "Noncovalent Interaction": A Chemical Misnomer That Inhibits Proper Understanding of Hydrogen Bonding, Rotation Barriers, and Other Topics, Molecules 28 (9) (2023) 3776.

[25] F. Hussain, R. Hussain, M. Adnan, S. Muhammad, Z. Irshad, M.U. Khan, K. Ayub, Insights into the nonlinear optical (NLO) response of pure Aum (2≥ m≤ 7) and copper-doped Au m–x Cu x clusters, RSC Adv. 12 (39) (2022) 25143–25153.

[26] G.Y. Li, G.J. Zhao, Y.H. Liu, K.L. Han, G.Z. He, TD-DFT study on the sensing mechanism of a fluorescent chemosensor for fluoride: Excited-state proton transfer, J. Comput. Chem. 31 (8) (2010) 1759–1765.

[27] Lu, T., & Chen, Q. (2021). mwfn: A strict, concise and extensible format for electronic wavefunction storage and exchange.

[28] Z. Zheng, X. Zu, Y. Zhang, W. Zhou, Rational design of type-II nano-heterojunctions for nanoscale optoelectronics, Materials Today Physics 15 (2020) 100262.

[29] M.G. Chiariello, N. Rega, Exploring nuclear photorelaxation of pyranine in aqueous solution: An integrated ab-initio molecular dynamics and time resolved vibrational analysis approach, The Journal of Physical Chemistry A 122 (11) (2018) 2884–2893.

[30] A. Mohamadzade, S. Ullrich, Internal conversion and intersystem crossing dynamics of uracil upon double thionation: a time-resolved photoelectron spectroscopy study in the gas phase, PCCP 22 (27) (2020) 15608–15615.

[31] A.D. Bochevarov, E. Harder, T.F. Hughes, J.R. Greenwood, D.A. Braden, D. M. Philipp, R.A. Friesner, Jaguar: A high-performance quantum chemistry software program with strengths in life and materials sciences, Int. J.of Quantum Chemistry 113 (18) (2013) 2110–2142.

[32] P. Hess, Bonding, structure, and mechanical stability of 2D materials: the predictive power of the periodic table, Nanoscale Horiz. 6 (11) (2021) 856–892.

[33] A.R. Ayub, M. Ilyas, N. Hassan, K. Irshad, M. Zeshan, S. Arshad, J. Iqbal, Host-guest coupling to potentially increase the bio-accessibility of 1-(2-chloroethyl)-3-cyclohexyl-1-nitrosourea by nanocarrier graphyne for brain tumor therapy, a comprehensive quantum mechanics study, J. Mol. Graph. Model. 123 (2023) 108517.

[34] I. Salahshoori, M.N. Jorabchi, S. Ghasemi, M. Golriz, S. Wohlrab, H.A. Khonakdar, An in silico study of sustainable drug pollutants removal using carboxylic acid functionalized-MOF nanostructures (MIL-53 (Al)-(COOH) 2): Towards a greener future, Desalination 559 (2023) 116654.

[35] N.H. Kazim, L.H. Khadim, Study of Suggested Chemotherapy Agent of bis ((S)-3-methoxycarbamoyl pentanoate) di chloride bis (ethyl amine) platinum (IV)) MPP) using DFT, Egypt. J. Chem. 64 (7) (2021) 3405–3411.

[36] R. Hayes, G.G. Warr, R. Atkin, Structure and nanostructure in ionic liquids, Chem. Rev. 115 (13) (2015) 6357–6426.

[37] F. Weinhold, C.R. Landis, Valency and bonding: a natural bond orbital donor-acceptor perspective, Cambridge University Press, 2005.

[38] A. Thamarai, R. Vadamalar, M. Raja, S. Muthu, B. Narayana, P. Ramesh, S. Aayisha, Molecular structure interpretation, spectroscopic (FT-IR, FT-Raman), electronic solvation (UV–Vis, HOMO-LUMO and NLO) properties and biological evaluation of (2E)-3-(biphenyl-4-yl)-1-(4-bromophenyl) prop-2-en-1-one: Experimental and computational modeling approach, Spectrochim. Acta A Mol. Biomol. Spectrosc. 226 (2020) 117609.

[39] J.E. Šponer, R. Szabla, R.W. Góra, A.M. Saitta, F. Pietrucci, F. Saija, J. Šponer, Prebiotic synthesis of nucleic acids and their building blocks at the atomic level–merging models and mechanisms from advanced computations and experiments, PCCP 18 (30) (2016) 20047–20066.

[40] F. Feixas, E. Matito, J. Poater, M. Solà, Quantifying aromaticity with electron delocalisation measures, Chem. Soc. Rev. 44 (18) (2015) 6434–6451.

[41] J.B. Martins, Electron dynamics in organic molecules by Core-Hole Clock spectroscopy, Sorbonne Université), 2021. Doctoral dissertation.

[42] R. Ravisankar, P. Jayaprakash, P. Eswaran, K. Mohanraj, G. Vinitha, M. Pichumani, Synthesis, growth, optical and third-order nonlinear optical properties of glycine sodium nitrate single crystal for photonic device applications, J. Mater. Sci. Mater. Electron. 31 (2020) 17320–17331.

[43] S. Muthu, G. Ramachandran, Spectroscopic studies (FTIR, FT-Raman and UV–Visible), normal coordinate analysis, NBO analysis, first order hyper polarizability, HOMO and LUMO analysis of (1R)-N-(Prop-2-yn-1-yl)-2, 3-dihydro-1H-inden-1-amine molecule by ab initio HF and density functional methods, Spectrochim. Acta A Mol. Biomol. Spectrosc. 121 (2014) 394–403.

[44] Z. Liu, T. Lu, Q. Chen, An sp-hybridized all-carboatomic ring, cyclo [18] carbon: Electronic structure, electronic spectrum, and optical nonlinearity, Carbon 165 (2020) 461–467.

[45] P.C. Ray, Size and shape dependent second order nonlinear optical properties of nanomaterials and their application in biological and chemical sensing, Chem. Rev. 110 (9) (2010) 5332–5365.

[46] G. Bharathy, J.C. Prasana, S. Muthu, A. Irfan, F.B. Asif, A. Saral, S. Aayisha, Evaluation of electronic and biological interactions between N-[4-(Ethylsulfamoyl) phenyl] acetamide and some polar liquids (IEFPCM solvation model) with Fukui function and molecular docking analysis, J. Mol. Liq. 340 (2021) 117271.

[47] M. Sumithra, S.J. Pradeepa, D. Tamilvendan, M.S. Boobalan, N. Sundaraganesan, Spectral (FT-IR, FT-Raman, NMR, UV–vis), electronic structure (DFT, TD-DFT), and molecular docking investigations on 1-((1H-benzo [d] imidazol-1-yl) methyl) urea–A bioactive Mannich base system, Chem. Phys. Lett. 806 (2022) 140047.

[48] N. Hou, F.Y. Du, H.S. Wu, Effects of Li doping and B3N3 substitution on the static first hyperpolarizabilities of biphenylene nanosheets: A computational and comparative study, Org. Electron. 68 (2019) 9–14.

[49] T.J. Penfold, E. Gindensperger, C. Daniel, C.M. Marian, Spin-vibronic mechanism for intersystem crossing, Chem. Rev. 118 (15) (2018) 6975–7025.

[50] Y. Wen, H. Ding, Y. Shan, Preparation and visible light photocatalytic activity of Ag/TiO 2/graphene nanocomposite, Nanoscale 3 (10) (2011) 4411–4417.

[51] R. Trusovas, G. Račiukaitis, G. Niaura, J. Barkauskas, G. Valušis, R. Pauliukaite, Recent advances in laser utilization in the chemical modification of graphene oxide and its applications, Adv. Opt. Mater. 4 (1) (2016) 37–65.

[52] A.G. Pramod, Y.F. Nadaf, C.G. Renuka, Synthesis, photophysical, quantum chemical investigation, linear and non-linear optical properties of coumarin derivative: Optoelectronic and optical limiting application, Spectrochim. Acta A Mol. Biomol. Spectrosc. 223 (2019) 117288.

[53] Y.C. Hung, J.C. Jiang, C.Y. Chao, W.F. Su, S.T. Lin, Theoretical Study on the Correlation between Band Gap, Bandwidth, and Oscillator Strength in Fluorene-Based Donor− Acceptor Conjugated Copolymers, J. Phys. Chem. B 113 (24) (2009) 8268–8277.

[54] Y. Ozaki, Y. Morisawa, I. Tanabe, K.B. Beć, ATR-far-ultraviolet spectroscopy in the condensed phase—The present status and future perspectives, Spectrochim. Acta A Mol. Biomol. Spectrosc. 253 (2021) 119549.

[55] H. Li, Y. Zhou, Y. Liu, L. Li, Y. Liu, Q. Wang, Dielectric polymers for high-temperature capacitive energy storage, Chem. Soc. Rev. 50 (11) (2021) 6369–6400.

[56] P. Mahalingavelar, How End-Capped Acceptors Regulate the Photovoltaic Performance of the Organic Solar Cells: A Detailed Density Functional Exploration of Their Impact on the A-D− π–D–A Type Small Molecular Electron Donors, Energy Fuel 36 (4) (2022) 2095–2107.

[57] K. Kloss, influence of the dielectric substrate on the electronic band structure in a monolayer of tmdc (Doctoral dissertation, Université Grenoble Alpes (2022) [2020-....].

[58] P. Cui, Y. Xue, Edge carboxylation-induced charge separation dynamics of graphene quantum dot/cellulose nanocomposites, Carbohydr. Polym. 299 (2023) 120190.

[59] Y. Zhang, C. Shen, X. Lu, X. Mu, P. Song, Effects of defects in g-C3N4 on excited-state charge distribution and transfer: Potential for improved photocatalysis, Spectrochim. Acta A Mol. Biomol. Spectrosc. 227 (2020) 117687.

[60] A.D. Isravel, J.K. Jeyaraj, S. Thangasamy, W.J. John, DFT, NBO, HOMO-LUMO, NCI, stability, Fukui function and hole–Electron analyses of tolcapone, Comput. Theor. Chem. 1202 (2021) 113296.

[61] W. Liu, Q. Liu, C. Xiang, H. Zhou, L. Jiang, Y. Zou, Theoretical exploration of optoelectronic performance of PM6: Y6 series-based organic solar cells, Surf. Interfaces 26 (2021) 101385.

[62] F.M. Rombach, S.A. Haque, T.J. Macdonald, Lessons learned from spiro-OMeTAD and PTAA in perovskite solar cells, Energ. Environ. Sci. 14 (10) (2021) 5161–5190.

[63] Z. Mahimwalla, K.G. Yager, J.I. Mamiya, A. Shishido, A. Priimagi, C.J. Barrett, Azobenzene photomechanics: prospects and potential applications, Polym. Bull. 69 (2012) 967–1006.
[64] Y. Wang, G.H. Robinson, Unique homonuclear multiple bonding in main group compounds, Chem. Commun. 35 (2009) 5201–5213.
[65] L. Zhang, W. Shen, R. He, X. Liu, X. Tang, Y. Yang, M. Li, Fine structural tuning of diketopyrrolopyrrole-cored donor materials for small molecule-fullerene organic solar cells: a theoretical study, Org. Electron. 32 (2016) 134–144.
[66] T. Nelson, S. Fernandez-Alberti, A.E. Roitberg, S. Tretiak, Nonadiabatic excited-state molecular dynamics: Modeling photophysics in organic conjugated materials, Acc. Chem. Res. 47 (4) (2014) 1155–1164.
[67] S. Sett, A. Parappurath, N.K. Gill, N. Chauhan, A. Ghosh, Engineering sensitivity and spectral range of photodetection in van der Waals materials and hybrids, Nano Express 3 (1) (2022) 014001.
[68] F. Labat, I. Ciofini, H.P. Hratchian, M.J. Frisch, K. Raghavachari, C. Adamo, Insights into working principles of ruthenium polypyridyl dye-sensitized solar cells from first principles modeling, J. Phys. Chem. C 115 (10) (2011) 4297–4306.
[69] K. Pei, Y. Wu, W. Wu, Q. Zhang, B. Chen, H. Tian, W. Zhu, Constructing Organic D-A–π-A-Featured Sensitizers with a Quinoxaline Unit for High-Efficiency Solar Cells: The Effect of an Auxiliary Acceptor on the Absorption and the Energy Level Alignment. Chemistry–A, European Journal 18 (26) (2012) 8190–8200.
[70] J. George, J.C. Prasana, S. Muthu, T.K. Kuruvilla, S. Sevanthi, R.S. Saji, Spectroscopic (FT-IR, FT Raman) and quantum mechanical study on N-(2, 6-dimethylphenyl)-2-{4-[2-hydroxy-3-(2-methoxyphenoxy) propyl] piperazin-1-yl} acetamide, J. Mol. Struct. 1171 (2018) 268–278.
[71] A. Azaid, M. Raftani, M. Alaqarbeh, R. Kacimi, T. Abram, Y. Khaddam, M. Bouachrine, New organic dye-sensitized solar cells based on the D-A–π–A structure for efficient DSSCs: DFT/TD-DFT investigations, RSC Adv. 12 (47) (2022) 30626–30638.
[72] M. Raftani, T. Abram, A. Azaid, R. Kacimi, M.N. Bennani, M. Bouachrine, New organic dyes with low bandgap based on heterocyclic compounds for dye-sensitized solar cells applications. Biointerface Research in Applied, Chemistry 13 (2023).